Inorganic Chemistry

Article

pubs.acs.org/IC

Evaluation of ^{95}Mo Nuclear Shielding and Chemical Shift of $[Mo_6X_{14}]^{2-}$ Clusters in the Liquid Phase

Thi Thuong Nguyen,[†] Julie Jung,[†] Xavier Trivelli,[‡] Julien Trébosc,[§] Stéphane Cordier,[†] Yann Molard,[†] Laurent Le Pollès,[†] Chris J. Pickard,[∥] Jérôme Cuny,*[,⊥] and Régis Gautier*[,†]

[†]Institut des Sciences Chimiques de Rennes, UMR 6226 CNRS—Université de Rennes 1-Ecole Nationale Supérieure de Chimie de Rennes, 11 Allée de Beaulieu, 35708 Rennes, France

[‡]Unité de Glycobiologie Structurale et Fonctionnelle, UMR 8576 CNRS—Université Lille 1, IFR 147, Cité Scientifique Bâtiment C9, 59655 Villeneuve d'Ascq, France

[§]Unité de Catalyse et Chimie du Solide, UMR 8181 CNRS—Université de Lille 1, 59655 Villeneuve d'Ascq, France

[∥]Department of Physics and Astronomy, University College London, Gower Street, London WC1E6BT, United Kingdom

[⊥]Laboratoire de Chimie et Physique Quantiques (LCPQ), Université de Toulouse III [UPS] and CNRS, 118 Route de Narbonne, F-31062 Toulouse, France

Supporting Information

ABSTRACT: $[Mo_6X_{14}]^{2-}$ octahedral molybdenum clusters are the main building blocks of a large range of materials. Although ^{95}Mo nuclear magnetic resonance was proposed to be a powerful tool to characterize their structural and dynamical properties in solution, these measurements have never been complemented by theoretical studies which can limit their interpretation for complex systems. In this Article, we use quantum chemical calculations to evaluate the ^{95}Mo chemical shift of three clusters: $[Mo_6Cl_{14}]^{2-}$, $[Mo_6Br_{14}]^{2-}$, and $[Mo_6I_{14}]^{2-}$. In particular, we test various computational parameters influencing the quality of the results: size of the basis set, treatment of relativistic and solvent effects. Furthermore, to provide quantum chemical calculations that are directly comparable with experimental data, we evaluate for the first time the ^{95}Mo nuclear magnetic shielding of the experimental reference, namely, MoO_4^{2-} in aqueous solution. This is achieved by combining ab initio molecular dynamics simulations with a periodic approach to evaluate the ^{95}Mo nuclear shieldings. The results demonstrate that, despite the difficulty to obtain accurate ^{95}Mo chemical shifts, relative values for a cluster series can be fairly well-reproduced by DFT calculations. We also show that performing an explicit solvent treatment for the reference compound improves by ∼50 ppm the agreement between theory and experiment. Finally, the standard deviation of ∼70 ppm that we calculate for the ^{95}Mo nuclear shielding of the reference provides an estimation of the accuracy we can achieve for the calculation of the ^{95}Mo chemical shifts using a static approach. These results demonstrate the growing ability of quantum chemical calculations to complement and interpret complex experimental measurements.

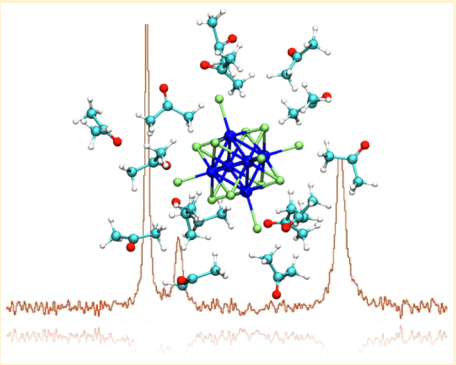

INTRODUCTION

Synthesis, structural characterization, and processing of new materials is a subject of major importance in modern chemistry. Thus, over past decades, an ongoing effort has been devoted to the development of various classes of materials displaying original physical properties. Among them, a rich inorganic chemistry based on molybdenum clusters has been developed.[1−3] Its quick expansion is related to the discovery of the high critical field superconductor properties (∼60 T) of the $PbMo_6S_8$-type phases prepared by Chevrel and Sergent.[4] From that time, a large variety of compounds based on molybdenum clusters has been synthesized that present, among other properties, molecular magnetism,[5,6] luminescence,[7] and thermoelectric properties.[8−11] More recently, the use of soft-synthesis routes has allowed for the development of new nanomaterials and hybrid organic−inorganic structures incorporating molybdenum clusters and thus acquiring their peculiar physical properties.[12,13] For example, the luminescence properties of the $[Mo_6X^i_8X^a_6]^{2-}$ octahedral cluster (see Figure 1 for the structure of this motif and the definition of X^i and X^a positions), where X stands for an halogen, can be incorporated into silica nanoparticles,[14−17] adsorbed on ZnO nanocrystals,[15,18] in liquid crystal type materials,[19−22] and in polymers.[23−25] Once incorporated in a biocompatible medium, their large emission region in the red and near-infrared (wavelength range from 580 to 900 nm) makes them excellent candidates for applications in bioimagery and biolabeling.[14] They can also be used in the development of white light

Received: February 19, 2015
Published: July 24, 2015

DOI: 10.1021/acs.inorgchem.5b00396
Inorg. Chem. 2015, 54, 7673−7683

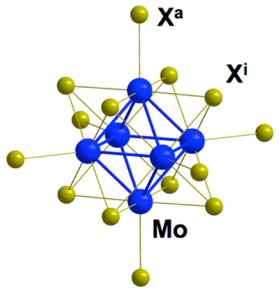

Figure 1. Structure of an octahedral $[Mo_6X^i_8X^a_6]^{2-}$ cluster where X stands for Cl, Br, or I; X^i for an inner ligand and X^a for an apical ligand. X and Mo atoms are represented by green and blue spheres, respectively.

emitting diodes,[18] luminescent solar cell concentrators,[26] photocatalysts,[27] and surface functionalization.[28,29]

The properties of such materials are very sensitive to the nature of the apical ligand of the molybdenum cluster. Indeed, to tune the affinity of the $[Mo_6X^i_8]$ metallic core with an organic or inorganic matrix, the X^a halogens can be replaced by suitable inorganic or functional organic ligands. This ligand exchange reaction is achieved in an aqueous or organic medium and can lead to a variety of isomers of chemically distinct species that are hardly separable. Thus, if we intend to get a better control on the preparation of new cluster based materials, it is of major importance to understand the atomic scale behavior of the $[Mo_6X^i_8X^a_6]^{2-}$ species. This requires an accurate characterization of their structural, dynamical, and ligand exchange properties in solution. As highlighted in the review by Preetz et al.,[30] the literature devoted to this specific subject is rich but mainly dominated by experimental works. In particular, ^{19}F nuclear magnetic resonance (NMR) spectroscopy has proved to be a specific and sensitive tool to characterize the structure and discriminate the various isomers in the series $[(Mo_6Cl^i_8)F^a_nY^a_{6-n}]^{2-}$, n = 1−6, Y = Cl, Br, and I,[31] and $[Mo_6(Cl^i_{8-n}Y^i_n)F^a_6]^{2-}$, n = 0−8, Y = Br and I.[32,33] In the former case, Dean−Evans-like relations exist for the three series between the number of fluorine apical ligands and the ^{19}F signals. Similar studies were also performed for tungsten and mixed tungsten/molybdenum clusters.[34]

These studies reveal that ligand exchange reactions on fluorinated metal clusters can easily be monitored by liquid state ^{19}F NMR. However, this becomes much more challenging for nonfluorinated species for which *J*-coupling informations are hardly extractable. Consequently, it is highly desirable to develop a tool that is general enough to handle all kinds of molybdenum clusters with equivalent accuracy and efficiency. A natural choice is ^{95}Mo NMR spectroscopy which was proposed by Harder et al. on the $[(Mo_6Cl^i_8)Y^a_6]^{2-}$, $[(Mo_6Br^i_8)Y^a_6]^{2-}$, and $[(Mo_6I^i_8)Y^a_6]^{2-}$ series (Y = F, Cl, Br, and I).[31,35] At that point, the application to more complex clusters was prevented as no theoretical tool was available to complement and interpret the experiments.

To fill in this gap, we propose in the present work to revisit the ^{95}Mo NMR measurements of the three octahedral $[Mo_6X_{14}]^{2-}$ clusters (X = Cl, Br, and I). By combining experimental results with quantum chemical calculations, we intend to develop an efficient and general tool for the structural characterization of molybdenum clusters. Our calculations of the ^{95}Mo NMR tensors are achieved in the framework of the density functional theory (DFT) for which we test the influence of various parameters: basis set size, inclusion of relativistic corrections, and solvent modeling. Furthermore, to be able to directly compare computational and experimental results, the theoretical evaluation of the ^{95}Mo NMR properties of a reference compound is also required. For molybdenum, the most commonly used experimental reference is an aqueous solution of MoO_4^{2-}. Despite the apparent simplicity of this species, its ^{95}Mo nuclear shielding is very complex to evaluate. Indeed, in addition to being influenced by the aforementioned computational parameters, the MoO_4^{2-} dianion strongly interacts with the surrounding solvent molecules. It is thus essential to treat them explicitly to accurately evaluate its ^{95}Mo nuclear shielding. Previous theoretical works on other metallic oxide anions already demonstrated such necessity.[36−41] Consequently, we performed an extensive *ab initio* molecular dynamics (AIMD) study of the MoO_4^{2-} ion in aqueous solution at various temperatures and with various initial conditions. Afterward, configurations along the trajectories were used to achieve both molecular and periodic quantum chemical calculations to get an average ^{95}Mo isotropic nuclear shielding value as converged as possible.

MATERIALS AND METHODS

Materials and NMR Spectroscopy. All solvents and 5 mm standard and 5 mm valve tubes were purchased from Euriso-top, Saint-Aubin, France. The three $(TBA)_2Mo_6X_{14}$ (X = Cl, Br, or I, and TBA = $(n\text{-}(C_4H_9)_4N)$) solid-state compounds were prepared according to the method described in the literature.[42] A saturated solution of each pure $(TBA)_2Mo_6X_{14}$ species was prepared in 0.6 mL of acetonitrile-d_3, as well as a mixed solution containing the three pure halides. A mixed solution containing 4.7 mg of $(TBA)_2Mo_6Cl_{14}$, 2.1 mg of $(TBA)_2Mo_6Br_{14}$, and 5.8 mg of $(TBA)_2Mo_6I_{14}$, resulting in a 6:2:4 molar ratio in 0.6 mL of acetone-d_6, was also prepared. Experiments were run at 300 K for all the acetonitrile-d_3 solutions and at 300 and 293 K for the acetone-d_6 solutions.

NMR experiments were performed on Bruker 9.4 T Avance I 400 and 21.1 T Avance III 900 spectrometers equipped with 5 broad-band probes for which molybdenum-95 resonates at 26.2 and 58.9 MHz, respectively. Due to a limited excitation width, we were unable to simultaneously acquire the signals of the three clusters at 21.1 MHz. The results discussed in this paper are thus the ones obtained at 9.4 MHz. Experiments were acquired using a 0.5 s relaxation delay and 82 or 163 ms acquisition times. To suppress acoustic ringing, an echo pulse sequence was used with an echo delay of 50 μs.[43] The number of acquisition points used for the Fourier transform was adapted in order to improve the signal-to-noise ratio without degrading the resolution. This leads to 2.6−10 ms effective acquisition times. Due to the widths of the signals and the external referencing procedure we applied, an experimental uncertainty of 5 ppm is obtained for all the ^{95}Mo chemical shifts.

***Ab Initio* Simulations.** *Molecular Nuclear Magnetic Shielding Calculations.* Molecular DFT calculations were performed with the ADF package 2012.[44] Nonrelativistic (NR) and scalar relativistic (SR) calculations using the zeroth order regular approximation (ZORA) of the Dirac equation were carried out.[45−47] The influence of spin−orbit (SO) coupling was also tested in the framework of the ZORA approximation.[48] In a previous study devoted to the computation of ^{95}Mo NMR parameters, some of us showed that a frozen core approximation does not provide accurate results.[49] Thus, in the present study, only all-electron Slater-type orbital basis sets were considered for all atoms. TZP and TZ2P are all-electron triple-ζ basis sets including one and two polarization functions for all atoms, respectively. QZ4P is an all-electron quadruple-ζ basis set including four polarization functions. It is worth pointing out that these basis sets were successfully applied to similar studies devoted to the evaluation of the ^{195}Pt NMR tensor of platinum ionic complexes.[50,51] For all the calculations, we added extra diffuse functions in the density fitting procedure as used in the ADF package 2012. The exchange-

DOI: 10.1021/acs.inorgchem.5b00396
Inorg. Chem. 2015, 54, 7673−7683

correlation interaction was described within the generalized gradient approximation of Perdew, Burke, and Ernzerhof.[52] In Supporting Information, we provide a discussion on the potential influence of using other density functional in particular hybrid functionals. The ADF numerical integration factor was set to 6.0 for all calculations as a value of 8.0 does not lead to any significant variation of our results. Nuclear magnetic shielding tensors have been computed with the gauge-including atomic orbitals (GIAO) method.[53,54] The resulting isotropic nuclear shielding values (σ_{iso}) are discussed in the text. Solvent effects were included by means of the ADF implementation of the conductor-like screening model (COSMO)[55−57] using acetone (ϵ = 20.7), acetonitrile (ϵ = 37.5), or water (ϵ = 78.39) as model solvent. Acetone and acetonitrile were chosen in order to compare our results with experimental measurements and water in order to provide an upper limit to the solvent influence within the continuum solvation approach. ^{95}Mo quadrupolar coupling constants (C_Q) were evaluated using a quadrupolar moment for ^{95}Mo equal to −22 mb.

Molecular Dynamics Simulations. The AIMD simulations were performed within the Car−Parrinello formalism as implemented in the CPMD code.[58,59] Of course, the sensitivity of AIMD simulations with respect to the choice of the density functional is always a concern, in particular for aqueous systems.[60−65] In this study, despite the well-known failure of most GGA functionals to properly describe liquid water, we chose to use the PBE functional to enable a consistent comparison with previous calculations of ^{95}Mo NMR parameters of solid-state compounds.[49,66,67] The consequences of this choice are discussed in detail in Supporting Information where we present mean-square displacement curves and self-diffusion coefficients extracted from the simulations. Electronic wave functions and densities were expanded with a plane-wave basis set defined by an energy cutoff of 35 and 280 Ry, respectively. Valence−core interactions were described by use of ultrasoft pseudopotentials.[68−70] For Mo, the valence included the 4s, 4p, 4d, and 5s states. The Koelling−Harmon scalar relativistic formulation of the radial Schrödinger equation was solved for the initial all-electron calculation performed to construct the pseudopotentials.[71] The Brillouin zone integration was done at the Γ point only.

All simulations of MoO_4^{2-} are performed in a 12.459 Å cubic box containing 61 heavy water molecules and one MoO_4^{2-} ion which lead to the density of heavy water at ambient pressure and temperature. We kept this density equal for all the simulations and supposed negligible the error induced by neglecting the thermal dilatation of the liquid. To get a good statistical convergence of the calculated ^{95}Mo nuclear shielding, we ran three totally independent sets of simulations, each of them at several temperatures. The initial atomic configurations were generated from a simulation at 550 K using the TIP4P empirical force-field as implemented in DL-POLY 2.20,[72,73] from which we selected three independent configurations at 100 ps interval. The MoO_4^{2-} ion was then added in the simulations boxes which were further equilibrated for 15 ps at 450 K using AIMD in the canonical ensemble. This rather high temperature was chosen to ensure a liquid-like behavior of the simulations and to improve sampling which is necessary due to the high freezing point of PBE liquid water (see Supporting Information). The temperature of the system was controlled using a colored-nose Langevin thermostat especially designed for CPMD simulations and tuned to efficiently sample all the ionic frequencies of the system up to 2000 cm^{-1}.[74] For each set of simulations, the temperature was decreased progressively from 450 K to 400, 370, 340, and 310 K and equilibrated at each of these four temperatures during 10 ps before performing 15 ps of production run still in the canonical ensemble. All these simulations were conducted using a fictitious electron mass of 350 au and a time step of 5 au. These parameters avoid any drift in the fictitious kinetic energy of the electrons and allow a good energy conservation on the time-scale of the simulations. This protocol leads to three independent simulations per temperature.

The molecular structures used for the NMR calculations on the $[MoO_4(H_2O)_N]^{2-}$ (N = 8, 10, and 12) species were directly extracted from the AIMD trajectories by including the water molecules presenting the N shortest Mo−O distances.

Periodic Nuclear Magnetic Shielding Calculations. Nuclear shielding tensors were evaluated using the CASTEP 5.5.2 code.[75] For consistency with the AIMD simulations, we used the PBE functional to describe the exchange-correlation term. The core−valence interactions were described using ultrasoft pseudopotentials in combination with a 44 Ry energy cutoff and a 2 × 2 × 2 Monkhorst−Pack k-point grid for the sampling of the Brillouin zone. The GIPAW formalism was used to calculate the tensors from the pseudoelectronic density.[76,77] This method has proven to be successful for the study of a large range of periodic systems.[78,79]

RESULTS AND DISCUSSION

Experimental Results. The ^{95}Mo NMR spectra were recorded at 9.4 T on samples containing only one of the three clusters in acetonitrile-d_3: $[Mo_6Cl_{14}]^{2-}$, $[Mo_6Br_{14}]^{2-}$, or $[Mo_6I_{14}]^{2-}$, and then on a mixed solution. We observed that the chemical shifts were identical in both cases, isolated or in mixed solution, and we thus decided to focus our analysis on mixed solutions. In order to test the influence of the solvent, the measurements were also performed in acetone-d_6 at 293 K. The corresponding results are provided in Table 1. As can be seen, the molybdenum chemical shift decreases with the electronegativity of the ligand, with $[Mo_6Cl_{14}]^{2-}$ displaying a significantly more shielded signal than $[Mo_6Br_{14}]^{2-}$ and $[Mo_6I_{14}]^{2-}$. These results are in full accordance with previous measurements performed by Preetz and co-workers.[30] Solvent and temperature have some influence on the ^{95}Mo chemical shifts, which has already been described for the ^{99}Ru signal of organometallic species.[80,81] However, this influence is small as compared with the difference in chemical shift between the three species. Finally, when looking at the experiment performed in acetone-d_6, the signals display a significant narrowing of the half-height widths when going from chlorine (480 Hz) to iodine (190 Hz). This behavior is somewhat counterintuitive as one expects an increase of the line widths with the size of the ligand. This point is further discussed in the next section.

Table 1. Experimental ^{95}Mo Chemical Shifts (Expressed in ppm) for the Three $[Mo_6X_{14}]^{2-}$ Clusters Acquired at 9.4 T in Two Distinct Solvents[a]

	$[Mo_6Cl_{14}]^{2-}$	$[Mo_6Br_{14}]^{2-}$	$[Mo_6I_{14}]^{2-}$
acetonitrile-d_3 (300 K)	2934	3201	3261
acetone-d_6 (293 K)	2937 (480)	3203 (360)	3256 (190)

[a]The values are externally referenced relative to a 2.7 M solution of Na_2MoO_4 in D_2O at pH = 8. Half-height (expressed in Hz) widths measured at 9.4 T are given in parentheses.

^{95}Mo Nuclear Shielding and Chemical Shift of the $[Mo_6X_{14}]^{2-}$ Clusters. *Geometry Optimization of the Isolated Clusters.* As demonstrated in a number of studies,[66,78,79] the geometry used for the calculation of NMR properties has, at least, as much influence on the quality of the results than the computational parameters themselves. As demonstrated by Bühl et al.[38,39,41] and Autschbach et al.,[83,84] this influence is even more remarkable for transition metal chemical shifts in negatively charged complexes which turn out to be extremely sensitive to metal−ligand distances. We thus performed geometry optimizations of the three clusters using various sets of computational parameters: basis set, relativistic, and solvent effects. In a purely octahedral symmetry, the geometry of each cluster is fully described by only three distances: Mo−Mo, Mo−X^a, and Mo−X^i. These optimized distances are

DOI: 10.1021/acs.inorgchem.5b00396
Inorg. Chem. 2015, 54, 7673−7683

presented for $[Mo_6Cl_{14}]^{2-}$ in Table 2. Data for $[Mo_6Br_{14}]^{2-}$ and $[Mo_6I_{14}]^{2-}$ are provided in Supporting Information and display the same trends.

Table 2. Optimized Geometry of the $[Mo_6Cl_{14}]^{2-}$ Cluster Obtained Using Various Sets of Computational Parameters[a]

relativistic treatment	Mo−Mo (Å)	Mo−Cl^i (Å)	Mo−Cl^a (Å)
	TZP Basis Set		
NR	2.659 (2.648)	2.552 (2.539)	2.503 (2.544)
RS	2.664 (2.654)	2.539 (2.527)	2.480 (2.505)
SO	2.664 (2.654)	2.539 (2.528)	2.480 (2.504)
	TZ2P Basis Set		
NR	2.599 (2.589)	2.531 (2.516)	2.513 (2.560)
RS	2.618 (2.610)	2.505 (2.497)	2.464 (2.483)
SO	2.618 (2.610)	2.506 (2.497)	2.464 (2.483)
	QZ4P Basis Set		
NR	2.639 (2.631)	2.502 (2.495)	2.457 (2.476)
RS	2.626 (2.618)	2.497 (2.489)	2.450 (2.469)
SO	2.626 (2.618)	2.497 (2.490)	2.450 (2.469)
	Experimental[82]		
	2.605	2.470	2.450

[a]Implicit solvent (water) calculations are indicated between parentheses. The averaged experimental values are obtained from an X-ray analysis of the $Cu_2Mo_6Cl_{14}$ solid-state compound.[82]

The most striking feature of the data of Table 2 is that the results do not depend much on the computational parameters. In particular, although nonrelativistic calculations are slightly different and subject to basis set effects, the scalar relativistic calculations with or without spin−orbit corrections are almost identical, as expected for a closed-shell system for which SO coupling contributes to the energy only in order c^{-4}. In the latter, the TZ2P basis set provides geometries nearly equivalent to the quadruple-ζ one as the distance variations do not exceed 0.01 Å. These results also suggest that the TZP basis set is not good enough for the three studied clusters as it systematically overestimates the distances, especially the metal−metal one. It is noteworthy to mention that this failure is more pronounced for species with heavier halogens (see Tables S1 and S2 in Supporting Information). As observed experimentally in the $Cu_2Mo_6X_{14}$ crystal structures, Mo−Mo and Mo−X bond lengths increase with the size of the ligand. This trend is accurately reproduced by our TZ2P and QZ4P calculations.

Geometry optimizations using water as implicit solvent were also performed. Water was chosen as it provides an upper limit in a continuum approach for the solvent influence on the cluster geometries. As can be seen in Table 2, the influence of the implicit solvent is hardly visible on the Mo−Mo and Mo−Cl^i distances and is of the order of ∼0.02−0.03 Å on the Mo−Cl^a distances. It is expected that these latter are the most influenced by any solvent effect as the Cl^a are the most reachable atoms by the solvent molecules. It is also worth pointing out that the Mo−Cl^a distances always increase when including the solvent effects. Finally, relativistic calculations performed with the TZ2P and QZ4P basis sets, with or without implicit solvent, present distances quite close to the distances measured experimentally on the same cluster in the $Cu_2Mo_6X_{14}$ solid-state compounds. Although liquid and solid-state clusters would necessarily display structural differences, this agreement provides strong confidence in the present computational approach.

^{95}Mo Nuclear Shieldings of the Isolated Clusters. Two approaches are conceivable to carry out the ^{95}Mo isotropic nuclear shielding calculations from the previously discussed optimized geometries. In the first one, a unique reference structure is used for each compound. In the second one, the nuclear shielding calculations are performed using the same set of computational parameters used for the geometry optimization. We carried out both approaches, and we first present the results obtained using the former one. For each cluster, we used as reference structure the one obtained from the scalar relativistic optimization in combination with the QZ4P basis set and no implicit solvent effect. The corresponding ^{95}Mo isotropic shieldings are presented in Table 3. Since the TZP basis set fails to describe the structural parameters of the $[Mo_6X_{14}]^{2-}$ species, we did not consider it for the calculations of the NMR parameters.

Table 3. Computed Nuclear Magnetic Shielding for the Three $[Mo_6X_{14}]^{2-}$ Clusters Obtained from Different Sets of Computational Parameters[a]

	$[Mo_6Cl_{14}]^{2-}$		$[Mo_6Br_{14}]^{2-}$		$[Mo_6I_{14}]^{2-}$	
	TZ2P	QZ4P	TZ2P	QZ4P	TZ2P	QZ4P
NR	−3322	−3378	−3650	−3665	−3670	−3718
SR	−3128	−3177	−3478	−3512	−3611	−3669
SO	−2944	N.C.	−3294	N.C.	−3452	N.C.

[a]For each compound, a unique structure was used that was obtained from the geometry optimization performed using a scalar relativistic calculation in combination with the QZ4P basis set and no implicit solvent treatment. Data are given in ppm. The calculations marked as N.C. were too memory consuming to be carried out.

Table 3 shows that the heavier the halogen, the lower the ^{95}Mo nuclear shielding, as observed experimentally. This trend is not expected when substituting a chlorine ligand with a heavier halogen as the normal halogen dependence (NHD) is a shielding of the nucleus bound to the halogen as observed for example for the ^{95}Mo signal in the $[Mo(CO)_5X]^-$ series.[85] As discussed by Kaupp and co-workers,[86] the NHD on a given nucleus is mainly due to a one-bond spin−orbit shift caused by the heavy neighboring halogen. The authors also demonstrated that the magnitude of this shift strongly depends on the probed nucleus valence s-orbital contribution to the bonding with the halogen. In the present study, the observed inverse halogen dependence may be due to the low 5s character of the metal−halogen bond leading to a small spin−orbit contribution on the molybdenum nuclear shielding. This low 5s character is confirmed by the low occupation of the 5s Mo orbital according to Mulliken population analysis (between 0.13 and 0.30 electrons depending on the halogen atom).

Table 3 also shows that ^{95}Mo nuclear shieldings computed with the QZ4P basis set are always slightly lower (by ∼50 ppm) than the ones obtained with the less extended TZ2P basis set. Interestingly, the successive inclusion of scalar relativistic and spin−orbit coupling corrections shield the molybdenum atoms whereas the ordering and the differences between the three signals are almost conserved. These results are somewhat different from what occurs in heavier 5d elements as demonstrated by Truflandier et al.[50] In this study of the $[PtX_4]^{2-}$ and $[PtX_6]^{2-}$ platinum complexes, the authors showed that scalar and spin−orbit coupling contributions to the ^{195}Pt nuclear magnetic shielding are opposite, the former decreasing it whereas the latter increasing it. Furthermore, these

DOI: 10.1021/acs.inorgchem.5b00396
Inorg. Chem. 2015, 54, 7673−7683

contributions lead to large variations of the differences in nuclear shieldings by several hundreds of ppm. These differences with the present results are not completely unexpected as the weaker relativistic effects at the molybdenum center and the chemical similarity between the three clusters suppose that the relativistic effects on the molybdenum atoms would be equivalent from one species to the other. The only exception is observed for $[Mo_6I_{14}]^{2-}$ where the strong relativistic effects on the heavy iodine induce a somewhat different behavior of the molybdenum signal between the nonrelativistic and the scalar relativistic calculations, with the spin−orbit contribution, although slightly smaller, being qualitatively the same compared with those of the two other clusters.

^{95}Mo quadrupolar coupling constants of $[Mo_6Cl_{14}]^{2-}$, $[Mo_6Br_{14}]^{2-}$, and $[Mo_6I_{14}]^{2-}$ are computed to be 7.27, 5.50, and 3.77 MHz, respectively, at the TZ2P spin−orbit level of theory. The heavier the halogen, the smaller the quadrupolar coupling constant. This explains the counterintuitive experimental decrease of the line widths with the size of the ligand. Indeed, this demonstrates that the weaker quadrupolar coupling interaction dominates over the slower molecular motion induced by a heavier halogen.

Isotropic nuclear shieldings cannot be directly compared with any experimental isotropic chemical shift (δ_{iso}). However, differences between σ_{iso} can be compared with differences between δ_{iso} since a unique reference compound was used. Experimentally, the chlorine cluster presents a signal 267 ppm lower than the bromine cluster's signal, itself 60 ppm lower than the iodine cluster's one. The computed differences between σ_{iso} of $[Mo_6Cl_{14}]^{2-}$ and $[Mo_6Br_{14}]^{2-}$ range from 287 to 350 ppm whereas the ones between $[Mo_6Br_{14}]^{2-}$ and $[Mo_6I_{14}]^{2-}$ range from 20 to 158 ppm. These small discrepancies between the experimental and theoretical differences in nuclear shielding are not unexpected. Indeed, other theoretical works dealing with the evaluation of the NMR parameters of transition metal compounds, both 3d or 5d, display similar results. For example, the study carried out by Truflandier et al. on platinum anionic complexes displays errors of ∼50 ppm for $[PtX_6]^{2-}$ complexes and ∼150 ppm for $[PtX_4]^{2-}$ complexes.[50] Similarly, the studies by Bühl and coworkers on vanadates and on the $[Fe(CN)_6]^{4-}$ and $[Fe(CN)_5(NO)]^{2-}$ iron complexes display errors of the order of ∼70 and ∼60 pm, respectively.[36,38,39] So, in the light of the accuracy achieved in these studies, the present results compare quite well with the experimental values for both the TZ2P and QZ4P basis sets.

As discussed above, the ^{95}Mo isotropic nuclear shieldings were also computed for geometries optimized using the same set of computational parameters. The results are presented in Figure 2. Since TZ2P and QZ4P basis sets lead to very similar results in terms of optimized geometries and of computed NMR parameters (see Table 3), only calculations using the former are further discussed. The computed σ_{iso} values range from −4400 to −3100 ppm, which is significantly larger than the range given in Table 3. In particular, nonrelativistic values are at least 400 ppm lower than the ones computed at fixed geometry. Taking into account scalar relativistic and spin−orbit coupling corrections systematically increases these values, whatever the nature of the ligand. σ_{iso} differences of ∼400 ppm are computed between $[Mo_6Cl_{14}]^{2-}$ and $[Mo_6Br_{14}]^{2-}$, whereas $[Mo_6Br_{14}]^{2-}$ and $[Mo_6I_{14}]^{2-}$ display close shielding values (computed differences of 17 and 41 ppm for SR and SO calculations, respectively). It is worth pointing out that, in contrast to the data of Table 3, only the calculations based on the spin−orbit ZORA Hamiltonian lead to the correct ordering of the signals. This demonstrates the high sensitivity of σ_{iso} with respect to the geometry of the cluster and thus the difficulty to reach a perfect agreement with experimental data.

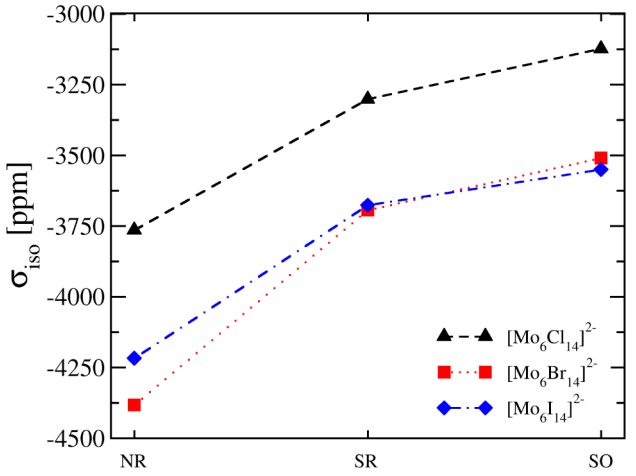

Figure 2. Computed isotropic nuclear magnetic shielding for the $[Mo_6X_{14}]^{2-}$ clusters using the TZ2P basis set. The geometries of each cluster were optimized with the same computational parameters used for the NMR calculation.

Since NMR experiments are carried out on liquid samples and we are considering charged species, solvation effects can play an important role in the computation of NMR tensors. They could in particular explain some of the discrepancies discussed above. Two main approaches allow ones to include these effects, namely, the explicit solvent treatment that we will present in the next section to study the MoO_4^{2-} ion in aqueous solution and the continuum solvation approach where the solute molecule is placed in a cavity of a continuous medium which simulates the sea of surrounding solvent molecules. This latter method requires much less computational effort and is more appropriate when the solute and the solvent do not directly interact through weak interactions such as hydrogen bonds. Thus, solvation effects were included in the calculations within this second approach using COSMO.[55−57] The influence of three model solvents, namely acetone, acetonitrile, and water, was tested on the geometries optimized in the gas phase. The results with the TZ2P basis set and the spin−orbit ZORA Hamiltonian are displayed in Figure 3. When solvent effects are included, all the computed ^{95}Mo σ_{iso} values increase by ∼100 ppm. Interestingly, the influence of the three model solvents is the same except for the iodine cluster in water, which is slightly more shielded that the one computed in acetone and acetonitrile. This similarity is consistent with the experimental results described above. Furthermore, the differences in the ^{95}Mo nuclear shielding remain almost the same, whatever the model solvent considered. The ^{95}Mo σ_{iso} were also computed including solvation effects on both geometries and NMR parameter calculations. Since COSMO has a very weak effect on the geometries, the resulting ^{95}Mo isotropic nuclear shielding constants do not differ much from the ones displayed in Figure 3.

^{95}Mo Chemical Shifts of the Isolated Clusters. In order to discuss our DFT results in terms of chemical shifts, one must first compute the nuclear shielding of the reference compound,

DOI: 10.1021/acs.inorgchem.5b00396
Inorg. Chem. 2015, 54, 7673−7683

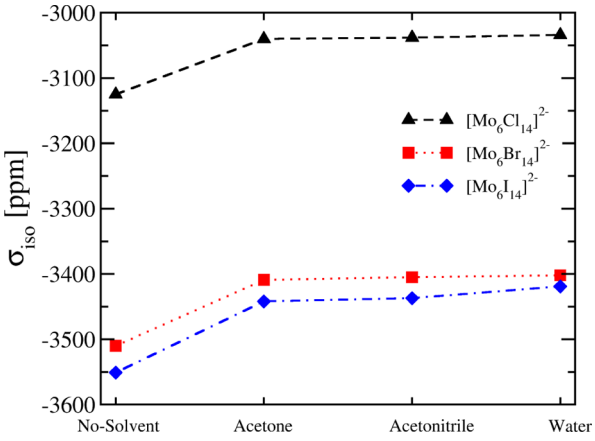

Figure 3. Computed ^{95}Mo isotropic nuclear magnetic shielding for the $[Mo_6X_{14}]^{2-}$ clusters for different model solvents using the TZ2P basis set and the spin−orbit ZORA Hamiltonian. The geometries were optimized using the same computational parameters but no solvent effect.

i.e. an aqueous solution of Na_2MoO_4. As a first attempt, the isotropic nuclear shielding of an isolated MoO_4^{2-} motif was evaluated using geometries optimized using the same computational parameters used to optimize the clusters. The Mo−O distance is hardly modified whatever the computational parameters considered: it varies from 1.787 to 1.818 Å. Using water as model solvent decreases the Mo−O distance by ∼0.01 Å. Figure 4 presents the ^{95}Mo δ_{iso} values computed using the following equation:

$$\delta_{iso}^{cluster} = -(\sigma_{iso}^{cluster} - \sigma_{iso}^{MoO_4^{2-}}) \quad (1)$$

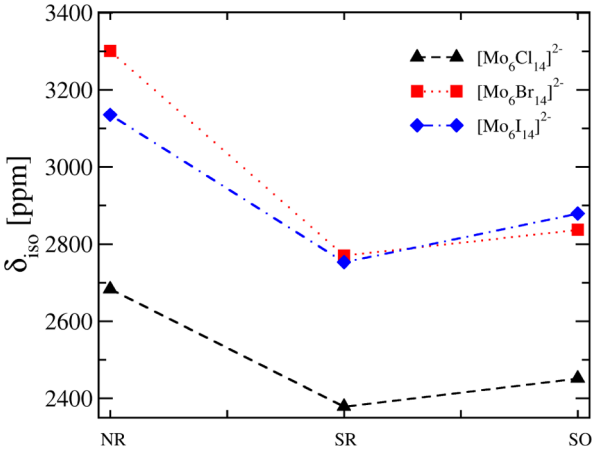

Figure 4. Computed ^{95}Mo isotropic chemical shift for the $[Mo_6X_{14}]^{2-}$ clusters using the TZ2P basis set without considering model solvent. The geometries of the clusters and of MoO_4^{2-} were optimized with the same computational parameters used for the NMR calculation.

The δ_{iso} range is significantly lower than the σ_{iso} one (see Figure 2), which demonstrates a partial cancellation of the relativistic contribution to the chemical shift between the clusters and the reference. We also evaluated the influence of solvation effects on the calculation of ^{95}Mo δ_{iso}. Figure 5 shows the results obtained using the TZ2P basis set and the spin−orbit ZORA Hamiltonian for the three model solvents. In this picture a unique nuclear shielding value of −675 ppm was used for MoO_4^{2-}, obtained by considering water as model solvent.

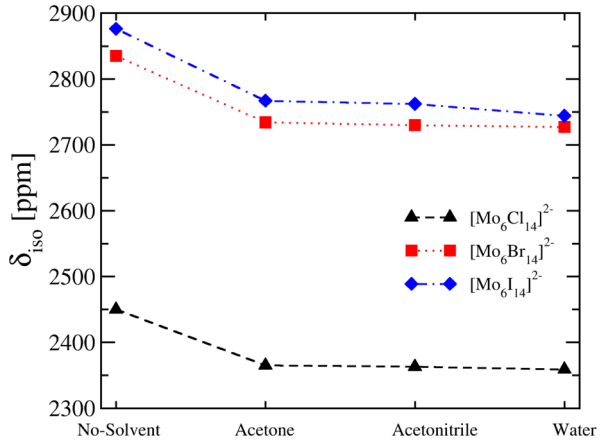

Figure 5. Computed ^{95}Mo isotropic chemical shifts for the $[Mo_6X_{14}]^{2-}$ clusters for different model solvents using the TZ2P basis set and the spin−orbit ZORA Hamiltonian. The geometries of the clusters and of MoO_4^{2-} were optimized using the same computational parameters but no solvent effect.

This leads to ^{95}Mo chemical shifts significantly too shielded as compared with the experimental values.

To summarize the first part of this work, we have shown that quantum chemical calculations are able to provide differences in ^{95}Mo isotropic nuclear shielding of $[Mo_6X_{14}]^{2-}$ clusters which compare quite well with experimental data. These results are achieved provided that extended enough basis sets are considered and that relativistic effects at the scalar or spin−orbit ZORA level of theory are included in the simulation. Modeling solvent effects with a continuum solvation approach such as COSMO influences the computed ^{95}Mo σ_{iso} by ∼100 ppm while differences in nuclear shielding between the clusters are conserved. However, the comparison between computed and experimental ^{95}Mo δ_{iso} is not straightforward due to the strong sensitivity of the results with respect to the computational parameters, geometries, and solvent effects. For example, the ^{95}Mo δ_{iso} of $[Mo_6Cl_{14}]^{2-}$ in acetone is computed to be ∼600 ppm lower than the experimental value. In addition to these sources of potential inaccuracies, discrepancies can also arise from an inaccurate evaluation of the ^{95}Mo nuclear shielding of the reference.

Computational Referencing Procedure of ^{95}Mo Chemical Shifts. Beyond the Continuum Solvation Model. In order to further examine the ability of computational approaches to compute chemical shifts, the effect of solvent on the calculation of the ^{95}Mo isotropic nuclear shielding of MoO_4^{2-} was studied in detail. To do so, as this species can strongly interact with solvent molecules, the ion−solvent interaction can hardly be neglected or described with an implicit solvation model as such an interaction is not taken into account in the model used in the first part of this work. Thus, we performed extensive *ab initio* molecular dynamics simulations to properly represent the solvated structure of MoO_4^{2-} and obtain a proper ensemble averaging of its ^{95}Mo nuclear shielding. This approach, already used for various kinds of transition metal species in aqueous solutions such as vanadates,[36,40] the permanganate ion,[37] iron cyanides,[38,39] and cobalt,[41] has proved to greatly enhance the accuracy of the theoretical evaluation of the corresponding chemical shifts. Thus, in this section, we focus our attention on the hydration structure of MoO_4^{2-} that will provide important knowledge to accurately evaluate its ^{95}Mo nuclear shielding.

DOI: 10.1021/acs.inorgchem.5b00396
Inorg. Chem. 2015, 54, 7673−7683

Structural Characterization of MoO_4^{2-} in Aqueous Solution. In Figure 6 are displayed the radial distribution

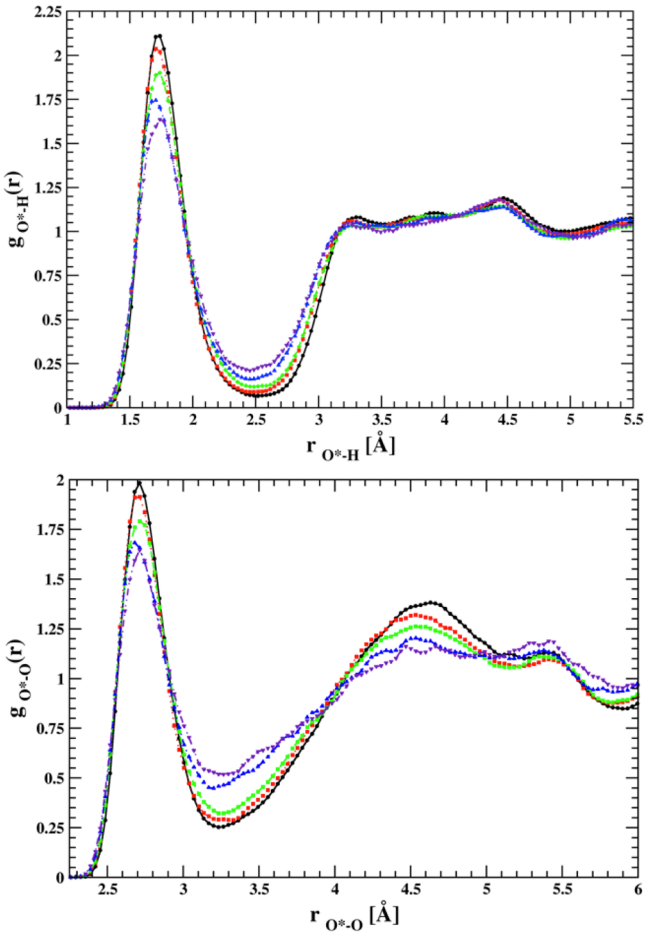

Figure 6. Radial distribution functions for O*−H (upper panel) and O*−O (lower panel) of MoO_4^{2-} in aqueous solution at 310 K (black plain line, circles), 340 K (red dotted line, square), 370 K (green dashed line, diamond), 400 K (blue dashed dotted line, triangle up), and 450 K (indigo dashed double dotted line, triangle down).

functions ($g(r)$'s) for O*−O and O*−H (O* stands for the oxygen atoms of MoO_4^{2-}) averaged over the three independent sets of AIMD simulations at five temperatures: 310, 340, 370, 400, and 450 K. At 310 K, the first peak of the two $g(r)$ is sharp and well-defined which reveals a strong interaction between MoO_4^{2-} and the surrounding water molecules. Furthermore, not only the first peak of the $g(r)$ functions is structured, but also the second one, which suggests that MoO_4^{2-} influences the medium up to the second solvation shell. This demonstrates the kosmotropic character of this species, similarly to sulfate or phosphate ions for example. Although slightly decreasing, the structure of the hydration shell remains even at 400 and 450 K.

When integrating the first peak of the two $g(r)$ functions at 310 K, we obtain an average coordination number per oxygen atom of 2.5, with average O*−O and O*−H distances equal to 2.70 and 1.72 Å, respectively. Thus, on average, the first hydration shell of MoO_4^{2-} encompasses 10 water molecules as displayed in Figure 7. Furthermore, it also appears from this picture that the hydration shell retains the tetrahedral shape of the ion. Thus, one can expect a strong angular anisotropy in the solvation shell of MoO_4^{2-} that disappears in the radial distribution functions due to the angular averaging. To

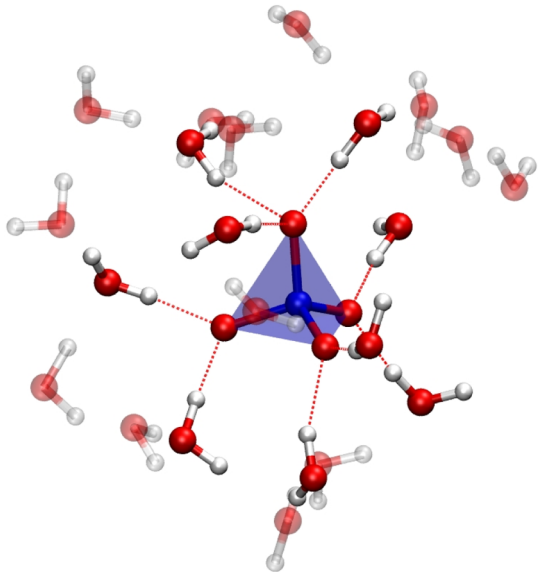

Figure 7. Representative snapshot of the hydrated structure of MoO_4^{2-} obtained from the present AIMD simulations. The water molecules in the first hydration shell are opaque whereas the farther ones are transparent.

demonstrate such property, we produced a three-dimensional density map of the localization of the oxygen and hydrogen atoms around MoO_4^{2-}. A selection of the corresponding isosurfaces is displayed in Figure 8. As shown in Figure 8A−C, each O* is surrounded by several water molecules in accordance with the $g(r)$ integration. However, these pictures show that these water molecules move on a disk centered around the Mo−O* axis. Thus, the first hydration shell presents clear cavities along these four axes as well as at the junction of the disks. Despite the poor statistical convergence of our surfaces at longer distance, it appears that the water molecules of the second hydration shell fill in these cavities, as displayed in Figure 8D.

All these results show the strong interaction of MoO_4^{2-} with the surrounding water molecules and the highly structured character of its hydration shell. This leads us to also look at the self-diffusion coefficient D_{self} of the water molecules in the simulations. These results are presented in Supporting Information. As already highlighted by Sit and Marzari,[87] PBE liquid water displays a frozen-like character at 310, 340, and 370 K whereas a liquid-like character is reached at 400 and 450 K. Of course, this has important implications for the statistical convergence of the calculation of the ^{95}Mo nuclear shielding of MoO_4^{2-} at 310, 340, and 370 K. Indeed, the frozen-like character of the simulations at these temperatures would certainly lead to a poor sampling of the phase space and to a less accurate ensemble averaging of the ^{95}Mo isotropic nuclear shielding. We partially overcome this weakness by averaging our results over three sets of independent simulations at each temperature. However, we also choose to consider the average ^{95}Mo isotropic nuclear shielding obtained at 400 K as more representative of the ambient temperature value as discussed further in the text.

Ensemble Averaging of the ^{95}Mo Nuclear Magnetic Shielding. From the various AIMD trajectories, we homogeneously selected 300 snapshots from which we evaluated the ^{95}Mo nuclear shielding of MoO_4^{2-} using the GIPAW approach.

DOI: 10.1021/acs.inorgchem.5b00396
Inorg. Chem. 2015, 54, 7673−7683

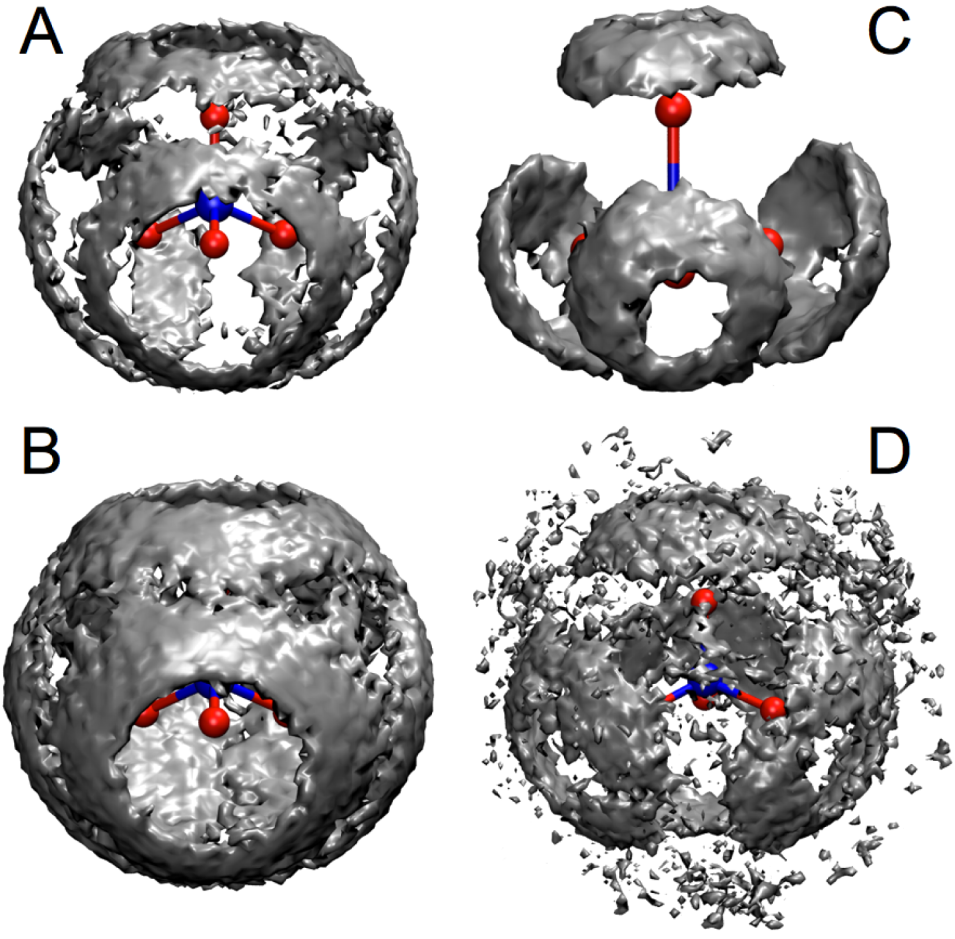

Figure 8. Three-dimensional density maps for the location of the oxygen (A, B, and D) and hydrogen (C) atoms around MoO_4^{2-} represented by different isosurfaces. A and B encompass only oxygen atoms in the first solvation shell whereas D also encompasses oxygen belonging to the second solvation shell. C includes only hydrogen atoms of the first solvation shell. To get a sufficient resolution, data coming from our simulations at 400 and 450 K were averaged.

The mean and standard deviation for each temperature and each set of simulations are gathered in Table 4.

Table 4. Mean (Roman) and Standard Deviation (Bold) for the MoO_4^{2-} ^{95}Mo Nuclear Magnetic Shielding Calculated from the Snapshots of the Three Sets of AIMD Simulations[a]

	310 K	340 K	370 K	400 K	450 K
first set	−870	−902	−892	−902	−895
	92	**66**	**86**	**103**	**106**
second set	−892	−898	−893	−896	−893
	79	**79**	**88**	**77**	**91**
third set	−873	−879	−899	−891	−910
	87	**79**	**106**	**87**	**103**
av per temp	−878	−893	−895	−896	−899

[a]All values are in ppm.

The means range from −910 to −870 ppm. If we assume that our data are statistically uncorrelated, the maximum standard deviation from the mean is 6 ppm and is obtained for the 450 K simulation of the first set. This rather low value shows that the ^{95}Mo nuclear shielding calculated for each simulation is well-converged. Thus, the dispersion of the results comes from the difficulty of a single simulation to properly explore the phase space due to the strong interaction of MoO_4^{2-} with its first two hydration shells and to the frozen-like character of the water molecules at 310, 340, and 370 K. This prevents each individual simulation from efficiently describing the phase space visited by the water molecules around MoO_4^{2-}. Consequently, a more accurate mean can be obtained at each temperature by averaging the values of the three sets of simulations as presented in Table 4. By doing so, one can observe a decrease of the ^{95}Mo nuclear shielding with the temperature. To the best of our knowledge, this dependence has not been observed experimentally. To confirm it, an accurate theoretical evaluation of this temperature gradient would require an averaging over many more simulations. Furthermore, as the PBE functional leads to a frozen-like liquid water, it would also be difficult to accurately connect a nuclear shielding value to a given temperature. Consequently, in the present study, we choose to consider the ^{95}Mo nuclear shielding computed at 400 K (−896 ppm) as the most representative of the ambient temperature value due to the liquid-like character of the water molecules at this temperature. It is worth pointing out that the averaged ^{95}Mo σ_{iso} values obtained at 340 K (−893 ppm) and 370 K (−895 ppm) are very close to the 400 K value although the simulations show a frozen-like behavior. Only the 310 K value is significantly different from the others, which highlights a wrong sampling of the system due to its strong frozen-like character.

DOI: 10.1021/acs.inorgchem.5b00396
Inorg. Chem. 2015, 54, 7673−7683

To use −896 ppm as a reference value for the ^{95}Mo nuclear magnetic shieldings, one has first to ascertain that the GIPAW calculations performed on MoO_4^{2-} have the same level of accuracy than the GIAO ones performed on the $[Mo_6X_{14}]^{2-}$ clusters. To do so, we selected from the 310 K simulation of the third set, 150 snapshots that were already used in the previous GIPAW calculations to design molecular clusters of general formula $[MoO_4(H_2O)_N]^{2-}$ (N = 8, 10, 12). These sizes were chosen since 10 is the average number of water molecules in the first hydration shell of MoO_4^{2-}; the values of 8 and 12 allow us to evaluate the influence of decreasing and increasing this number, respectively. The corresponding ^{95}Mo nuclear shieldings were evaluated using the scalar ZORA Hamiltonian in combination with the TZ2P basis set and are compared with the GIPAW results in Figure 9. Calculations for the

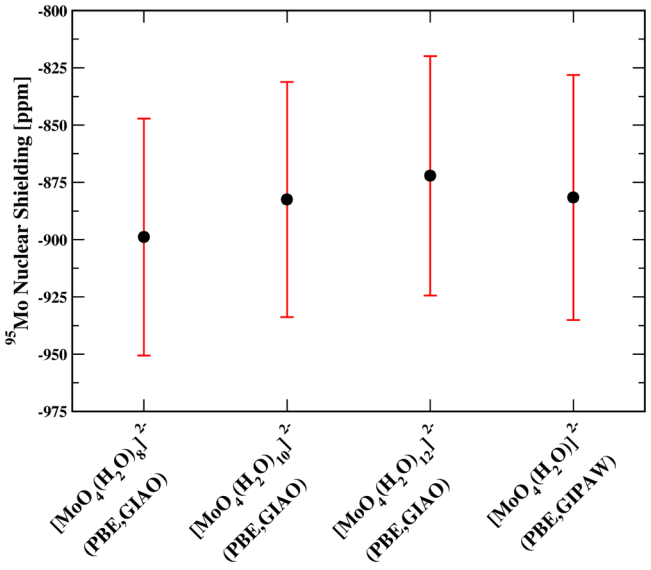

Figure 9. Mean (full circles) and standard deviation (bars) for the ^{95}Mo nuclear magnetic shielding calculated from 150 snapshots extracted from a molecular dynamics simulation performed at 310 K. Results are presented for the $[MoO_4(H_2O)_N]^{2-}$ (N = 8, 10, 12) clusters and the corresponding periodic structures.

$[MoO_4(H_2O)_{10}]^{2-}$ clusters were also performed using the spin−orbit ZORA Hamiltonian. When considering the SR calculations, both the mean nuclear shieldings and the standard deviation for the $[MoO_4(H_2O)_8]^{2-}$, $[MoO_4(H_2O)_{10}]^{2-}$, and $[MoO_4(H_2O)_{12}]^{2-}$ clusters and the periodic structures are very close. In particular, the average value for $[MoO_4(H_2O)_{10}]^{2-}$ displays only a ∼2 ppm difference with the periodic GIPAW calculations. This demonstrates that both approaches are equivalent, and thus, one can use −896 ppm as a good reference value for SR simulations. For SO calculations on the same $[MoO_4(H_2O)_{10}]^{2-}$ clusters, one obtains a mean and a standard deviation of −624 and 71 ppm, respectively. The former value allows us to shift the curves of Figure 5 by +51 ppm which improves by the same value the agreement between the chemical shifts calculated in acetone and acetonitrile as compared with the experimental values.

These results demonstrate that, in the case of a protic solvent, a gain in accuracy by ∼50 ppm can be reached for the calculation of ^{95}Mo chemical shifts by considering an explicit solvent description as compared with an implicit one. Despite this improvement, we obtain ^{95}Mo chemical shifts values of 2414, 2781, and 2813 ppm for $[Mo_6Cl_{14}]^{2-}$, $[Mo_6Br_{14}]^{2-}$, and $[Mo_6I_{14}]^{2-}$, respectively. This is approximatively 450 ppm too low as compared with the experimental values.

CONCLUSIONS

We provide in this contribution a complete study on the calculation of the ^{95}Mo isotropic nuclear shielding and chemical shift of $[Mo_6X_{14}]^{2-}$ (X = Cl, Br, I) species. The influence of basis set, relativistic, and solvent effects was tested. We demonstrate that, as far as relativistic effects are taken into account, a better agreement is reached between theory and experiment, at least for relative values of isotropic nuclear shieldings. Using a continuum solvation model influences the computed δ_{iso} by ∼100 ppm. Interestingly both calculated and measured ^{95}Mo δ_{iso} are not much influenced by the nature of the solvent. This suggests a weak solvent−solute interaction that we predict to be also true for strong dielectric solvent such as water. We also show that when an accurate study of the ^{95}Mo isotropic nuclear shielding of the reference compound is performed, an improvement of several tens of ppm is reached with respect to the experimental values. This demonstrates the need to explicitly describe the solvent water molecules in this case. Furthermore, the ∼70 ppm of standard deviation computed for the nuclear shielding of MoO_4^{2-} can be considered as a lower limit of accuracy for computed ^{95}Mo isotropic chemical shifts using a static approach. Large discrepancies still remain between theoretical and experimental ^{95}Mo isotropic chemical shifts. Several origins can be postulated, in particular the nature of the density functional used for the calculations (see Supporting Information). Another potential source of discrepancies is due to the fact that we did not take into account the thermal averaging of the ^{95}Mo nuclear shielding of the $[Mo_6X_{14}]^{2-}$ clusters. To do so, a study similar to the one achieved on the MoO_4^{2-} species would be required. Despite this limit, the present study demonstrates that first-principles calculations are interesting to complement complex ^{95}Mo NMR experimental measurements on molybdenum clusters in liquid phase.

ASSOCIATED CONTENT

Supporting Information

Optimized geometry of the $[Mo_6Br_{14}]^{2-}$ and $[Mo_6I_{14}]^{2-}$ clusters obtained using various sets of computational parameters and discussion on the nature of the density functional used for the calculations. Calculation and discussion of the self-diffusion coefficients of the water molecules in the first set of simulations. The Supporting Information is available free of charge on the ACS Publications website at DOI: 10.1021/acs.inorgchem.5b00396.

AUTHOR INFORMATION

Corresponding Authors

*Phone: +33 (0) 561556836. Fax: +33 (0) 561556065. E-mail: jerome.cuny@irsamc.ups-tlse.fr.

*E-mail: regis.gautier@ensc-rennes.fr

Notes

The authors declare no competing financial interest.

ACKNOWLEDGMENTS

The authors acknowledge Fernand Spiegelman for a critical reading of the manuscript and Karine Costuas for useful discussions. The authors are indebted to the Région Bretagne

DOI: 10.1021/acs.inorgchem.5b00396
Inorg. Chem. 2015, 54, 7673−7683

for a Ph.D. grant. Financial support from the TGIR-RMN-THC Fr3050 CNRS is gratefully acknowledged. The authors acknowledge support of the French Agence Nationale de la Recherche (ANR) under Grant NMRTHEO (ANR-09-JCJC-0088-01). The authors also thank the supercomputing facility of Toulouse III University, CALMIP, for the allocation of computer resources (P1320).

REFERENCES

(1) Chevrel, R.; Sergent, M. In *Topics in Current Physics*; Fischer, O., Maple, M., Eds.; Springer: Berlin, 1982; Vol. *32*, p 25.
(2) Simon, A. In *Clusters and Colloids—From Theory to Application*; Schmidt, G., Ed.; Verlag Chemie: New York, 1994; pp 373−458.
(3) Perrin, C. *J. Alloys Compd.* **1997**, *263*−*263*, 10.
(4) Chevrel, R.; Sergent, M.; Prigent, J. *J. Solid State Chem.* **1971**, *3*, 515−519.
(5) Peric, B.; Cordier, S.; Cuny, J.; Gautier, R.; Guizouarn, T.; Planinic, P. *Chem. - Eur. J.* **2011**, *17*, 6263−6271.
(6) Kirakci, K.; Cordier, S.; Shames, A.; Fontaine, B.; Hernandez, O.; Furet, E.; Halet, J.-F.; Gautier, R.; Perrin, C. *Chem. - Eur. J.* **2007**, *13*, 9608−9616.
(7) Maverick, A. W.; Gray, H. B. *J. Am. Chem. Soc.* **1981**, *103*, 1298−1300.
(8) Zhou, T.; Lenoir, B.; Colin, M.; Dauscher, A.; Al Rahal Al Orabi, R.; Gougeon, P.; Potel, M.; Guilmeau, E. *Appl. Phys. Lett.* **2011**, *98*, 162106.
(9) Gougeon, P.; Gall, P.; Al Rahal Al Orabi, R.; Fontaine, B.; Gautier, R.; Potel, M.; Zhou, T.; Lenoir, B.; Colin, M.; Candolfi, C.; Dauscher, A. *Chem. Mater.* **2012**, *24*, 2899−2908.
(10) Zhou, T.; Colin, M.; Candolfi, C.; Boulanger, C.; Dauscher, A.; Santava, E.; Hejtmanek, J.; Baranek, P.; Al Rahal Al Orabi, R.; Potel, M.; Fontaine, B.; Gougeon, P.; Gautier, R.; Lenoir, B. *Chem. Mater.* **2014**, *26*, 4765−4775.
(11) Al Rahal Al Orabi, R.; Gougeon, P.; Gall, P.; Fontaine, B.; Gautier, R.; Colin, M.; Candolfi, C.; Dauscher, A.; Hejtmanek, J.; Malaman, B.; Lenoir, B. *Inorg. Chem.* **2014**, *53*, 11699−11709.
(12) Cordier, S.; Kirakci, K.; Méry, D.; Perrin, C.; Astruc, D. *Inorg. Chim. Acta* **2006**, *359*, 1705−1709.
(13) Cordier, S.; Grasset, F.; Molard, Y.; Amela-Cortes, M.; Boukherroub, R.; Ravaine, S.; Mortier, M.; Ohashi, N.; Saito, N.; Haneda, H. *J. Inorg. Organomet. Polym. Mater.* **2015**, *25*, 189−204.
(14) Grasset, F.; Dorson, F.; Cordier, S.; Molard, Y.; Perrin, C.; Marie, A.-M.; Sasaki, T.; Haneda, H.; Bando, Y.; Mortier, M. *Adv. Mater.* **2008**, *20*, 143−148.
(15) Cordier, S.; Dorson, F.; Grasset, F.; Molard, Y.; Fabre, B.; Haneda, H.; Sasaki, T.; Mortier, M.; Ababou-Girard, S.; Perrin, C. *J. Cluster Sci.* **2009**, *20*, 9−21.
(16) Dechézelles, F.; Aubert, T.; Grasset, F.; Cordier, S.; Barthou, C.; Schwob, C.; Maître, A.; Vallée, R. A. L.; Cramail, H.; Ravaine, S. *Phys. Chem. Chem. Phys.* **2010**, *12*, 11993−11999.
(17) Aubert, T.; Cabello-Hurtado, F.; Esnault, M.-A.; Neaime, C.; Lebret-Chauvel, D.; Jeanne, S.; Pellen, P.; Roiland, C.; le Polles, L.; Saito, N.; Kimoto, K.; Haneda, H.; Ohashi, N.; Grasset, F.; Cordier, S. *J. Phys. Chem. C* **2013**, *117*, 20154−20163.
(18) Grasset, F.; Molard, Y.; Cordier, S.; Dorson, F.; Mortier, M.; Perrin, C.; Guilloux-Viry, M.; Sasaki, T.; Haneda, H. *Adv. Mater.* **2008**, *20*, 1710−1715.
(19) Molard, Y.; Dorson, F.; Cîrcu, V.; Roisnel, T.; Artzner, F.; Cordier, S. *Angew. Chem., Int. Ed.* **2010**, *49*, 3351−3355.
(20) Mocanu, A. S.; Amela-Cortes, M.; Molard, Y.; Circu, V.; Cordier, S. *Chem. Commun.* **2011**, *47*, 2056.
(21) Cortes, M. A.; Dorson, F.; Prévôt, M.; Ghoufi, A.; Fontaine, B.; Goujon, F.; Gautier, R.; Cîrcu, V.; Mériadec, C.; Artzner, F.; Folliot, H.; Cordier, S.; Molard, Y. *Chem. - Eur. J.* **2014**, *20*, 8561−8565.
(22) Nayak, S. K.; Amela-Cortes, M.; Roiland, C.; Cordier, S.; Molard, Y. *Chem. Commun.* **2015**, *51*, 3774−3777.
(23) Molard, Y.; Labbé, C.; Cardin, J.; Cordier, S. *Adv. Funct. Mater.* **2013**, *23*, 4821−4825.
(24) Garreau, A.; Massuyeau, F.; Cordier, S.; Molard, Y.; Gautron, E.; Bertoncini, P.; Faulques, E.; Wery, J.; Humbert, B.; Bulou, A.; Duvail, J.-L. *ACS Nano* **2013**, *7*, 2977−2987.
(25) Amela-Cortes, M.; Garreau, A.; Cordier, S.; Faulques, E.; Duvail, J.-L.; Molard, Y. J. *J. Mater. Chem. C* **2014**, *2*, 1545−1552.
(26) Zhao, Y.; Lunt, R. R. *Adv. Energy Mater.* **2013**, *3*, 1143−1148.
(27) Kumar, P.; Kumar, S.; Cordier, S.; Paofai, S.; Boukherroub, R.; Jain, S. L. *RSC Adv.* **2014**, *4*, 10420−10423.
(28) Ababou-Girard, S.; Cordier, S.; Fabre, B.; Molard, Y.; Perrin, C. *ChemPhysChem* **2007**, *8*, 2086−2090.
(29) Fabre, B.; Cordier, S.; Ababou-Girard, S.; Molard, Y.; Perrin, C.; Godet, C. *J. Phys. Chem. C* **2009**, *113*, 17437.
(30) Preetz, W.; Peters, G.; Bublitz, D. *Chem. Rev.* **1996**, *96*, 977−1026.
(31) Harder, K.; Peters, G.; Preetz, W. *Z. Anorg. Allg. Chem.* **1991**, *598*, 139−149.
(32) Brückner, P.; Peters, G.; Preetz, W. *Z. Anorg. Allg. Chem.* **1993**, *619*, 551−558.
(33) Brückner, P.; Peters, G.; Preetz, W. *Z. Anorg. Allg. Chem.* **1993**, *619*, 1920−1926.
(34) Brückner, P.; Peters, G.; Preetz, W. *Z. Anorg. Allg. Chem.* **1994**, *620*, 1669−1677.
(35) Preetz, W.; Bublitz, D.; von Schnering, H. G.; Saβümannshausen, J. *Z. Anorg. Allg. Chem.* **1994**, *620*, 234−246.
(36) Bühl, M.; Parrinello, M. *Chem. - Eur. J.* **2001**, *7*, 4487−4494.
(37) Bühl, M. *J. Phys. Chem. A* **2002**, *106*, 10505−10509.
(38) Bühl, M.; Mauschick, F. T. *Phys. Chem. Chem. Phys.* **2002**, *4*, 5508−5514.
(39) Bühl, M.; Mauschick, F. T.; Terstegen, F.; Wrackmeyer, B. *Angew. Chem., Int. Ed.* **2002**, *41*, 2312−2315.
(40) Bühl, M. *Inorg. Chem.* **2005**, *44*, 6277−6283.
(41) Bühl, M.; Grigoleit, S.; Kabrede, H.; Mauschick, F. T. *Chem. - Eur. J.* **2006**, *12*, 477−488.
(42) Kirakci, K.; Cordier, S.; Perrin, C. *Z. Anorg. Allg. Chem.* **2005**, *631*, 411−416.
(43) Brito, J. A.; Teruel, H.; Massou, S.; Gómez, M. *Magn. Reson. Chem.* **2009**, *47*, 573−577.
(44) te Velde, G.; Bickelhaupt, F. M.; Baerends, E. J.; Fonseca Guerra, C.; van Gisbergen, S. J. A.; Snijders, J. G.; Ziegler, T. *J. Comput. Chem.* **2001**, *22*, 931−967.
(45) van Lenthe, E.; Baerends, E. J.; Snijders, J. G. *J. Chem. Phys.* **1993**, *99*, 4597−4610.
(46) van Leeuwen, R.; van Lenthe, E.; Baerends, E. J.; Snijders, J. G. *J. Chem. Phys.* **1994**, *101*, 1272−1281.
(47) van Lenthe, E.; Baerends, E. J.; Snijders, J. G. *J. Chem. Phys.* **1994**, *101*, 9783−9792.
(48) Faas, S.; van Lenthe, J. H.; Hennum, A. C.; Snijders, J. G. *J. Chem. Phys.* **2000**, *113*, 4052−4059.
(49) Cuny, J.; Sykina, K.; Fontaine, B.; Le Polles, L.; Pickard, C. J.; Gautier, R. *Phys. Chem. Chem. Phys.* **2011**, *13*, 19471−19479.
(50) Truflandier, L. A.; Autschbach, J. *J. Am. Chem. Soc.* **2010**, *132*, 3472−3483.
(51) Truflandier, L. A.; Sutter, K.; Autschbach, J. *Inorg. Chem.* **2011**, *50*, 1723−1732.
(52) Perdew, J. P.; Burke, K.; Ernzerhof, M. *Phys. Rev. Lett.* **1996**, *77*, 3865−3868.
(53) Ditchfield, R. *J. Chem. Phys.* **1972**, *56*, 5688−5691.
(54) Wolinski, K.; Hinton, J. F.; Pulay, P. *J. Am. Chem. Soc.* **1990**, *112*, 8251−8260.
(55) Klamt, A.; Schuurmann, G. *J. Chem. Soc., Perkin Trans. 2* **1993**, 799−805.
(56) Klamt, A. *J. Phys. Chem.* **1995**, *99*, 2224−2235.
(57) Klamt, A.; Jonas, V. *J. Chem. Phys.* **1996**, *105*, 9972.
(58) Car, R.; Parrinello, M. *Phys. Rev. Lett.* **1985**, *55*, 2471−2474.
(59) *CPMD, version 3.15.1*; IBM Corporation: Armonk, New York, 1990−2008; MPI fr Festkrperforschung: Stuttgart, Germany, 1997−2001. http://www.cpmd.org.
(60) Sprik, M.; Hutter, J.; Parrinello, M. *J. Chem. Phys.* **1996**, *105*, 1142−1152.

DOI: 10.1021/acs.inorgchem.5b00396
Inorg. Chem. 2015, 54, 7673−7683

(61) Grossman, J. C.; Schwegler, E.; Draeger, E. W.; Gygi, F.; Galli, G. *J. Chem. Phys.* **2004**, *120*, 300−311.
(62) Schwegler, E.; Grossman, J. C.; Gygi, F.; Galli, G. *J. Chem. Phys.* **2004**, *121*, 5400−5409.
(63) VandeVondele, J.; Mohamed, F.; Krack, M.; Hütter, J.; Sprik, M.; Parrinello, M. *J. Chem. Phys.* **2005**, *122*, 014515 1−6.
(64) Izvekov, S.; Voth, G. A. *J. Chem. Phys.* **2005**, *123*, 044505 1−9.
(65) Hassanali, A. A.; Cuny, J.; Verdolino, V.; Parrinello, M. *Philos. Trans. R. Soc., A* **2014**, *372*, 20120482 1−32.
(66) Cuny, J.; Furet, E.; Gautier, R.; le Pollès, L.; Pickard, C. J.; d'Espinose de Lacaillerie, J.-B. *ChemPhysChem* **2009**, *10*, 3320−3329.
(67) Cuny, J.; Cordier, S.; Perrin, C.; Pickard, C. J.; Delevoye, L.; Trébosc, J.; Gan, Z.; Pollès, L. L.; Gautier, R. *Inorg. Chem.* **2013**, *52*, 617−627.
(68) Vanderbilt, D. *Phys. Rev. B: Condens. Matter Mater. Phys.* **1990**, *41*, 7892−7895.
(69) Laasonen, K.; Car, R.; Lee, C.; Vanderbilt, D. *Phys. Rev. B: Condens. Matter Mater. Phys.* **1991**, *43*, 6796−6799.
(70) Laasonen, K.; Pasquarello, A.; Car, R.; Lee, C.; Vanderbilt, D. *Phys. Rev. B: Condens. Matter Mater. Phys.* **1993**, *47*, 10142−10153.
(71) Koelling, D. D.; Harmon, B. N. *J. Phys. C: Solid State Phys.* **1977**, *10*, 3107−3114.
(72) Jorgensen, W. L.; Chandrasekhar, J.; Madura, J. D.; Impey, R. W.; Klein, M. L. *J. Chem. Phys.* **1983**, *79*, 926−935.
(73) Smith, W.; Forester, T. R. *J. Mol. Graphics* **1996**, *14*, 136−141.
(74) Ceriotti, M.; Bussi, G.; Parrinello, M. *Phys. Rev. Lett.* **2009**, *102*, 020601.
(75) Segall, M. D.; Lindan, P. J. D.; Probert, M. J.; Pickard, C. J.; Hasnip, P. J.; Clark, S. J.; Payne, M. C. *J. Phys.: Condens. Matter* **2002**, *14*, 2717.
(76) Pickard, C. J.; Mauri, F. *Phys. Rev. B: Condens. Matter Mater. Phys.* **2001**, *63*, 245101.
(77) Yates, J. R.; Pickard, C. J.; Mauri, F. *Phys. Rev. B: Condens. Matter Mater. Phys.* **2007**, *76*, 024401.
(78) Charpentier, T. *Solid State Nucl. Magn. Reson.* **2011**, *40*, 1−20.
(79) Bonhomme, C.; Gervais, C.; Babonneau, F.; Coelho, C.; Pourpoint, F.; Thierry, A.; Ashbrook, S. E.; Griffin, J. M.; Yates, J. R.; Mauri, F.; Pickard, C. J. *Chem. Rev.* **2012**, *112*, 5733−5779.
(80) Brevard, C.; Granger, P. *Inorg. Chem.* **1983**, *22*, 532−535.
(81) Gaemers, S.; van Slageren, J.; O'Connor, C. M.; Vos, J. G.; Hage, R.; Elsevier, C. J. *Organometallics* **1999**, *18*, 5238−5244.
(82) Peppenhorst, A.; Keller, H.-L. Z. *Z. Anorg. Allg. Chem.* **1996**, *622*, 663−669.
(83) Le Guennic, B.; Matsumoto, K.; Autschbach, J. *Magn. Reson. Chem.* **2004**, *42*, S99−S116.
(84) Autschbach, J.; le Guennic, B. *Chem. - Eur. J.* **2004**, *10*, 2581−2589.
(85) John, M. *Annu. Rep. NMR Spectrosc.* **1996**, *33*, 151−206.
(86) Kaupp, M.; Malkina, O. L.; Malkin, V. G.; Pyykkö, P. *Chem. - Eur. J.* **1998**, *4*, 118−126.
(87) Sit, P. H.-L.; Marzari, N. *J. Chem. Phys.* **2005**, *122*, 204510.

DOI: 10.1021/acs.inorgchem.5b00396
Inorg. Chem. 2015, 54, 7673−7683